



Self-supported nanoporous cobalt phosphosulfate electrodes for efficient hydrogen evolution reaction



Wenting Hong^{a,b}, Chuanyong Jian^a, Genxiang Wang^{a,b}, Xu He^a, Jing Li^a, Qian Cai^a, Zhenhai Wen^{a,c}, Wei Liu^{a,c,*}

^a CAS Key Laboratory of Design and Assembly of Functional Nanostructures, Fujian Provincial Key Laboratory of Nanomaterials, Fujian Institute of Research on the Structure of Matter, Chinese Academy of Sciences, Fuzhou, 350002, China

^b University of Chinese Academy of Sciences, Beijing, 100049, China

^c Fujian Provincial Key Laboratory of Nanomaterials, Fujian Institute of Research on the Structure of Matter, Chinese Academy of Sciences, Fuzhou, 350002, China

ARTICLE INFO

Keywords:

Nanoporous
Cobalt phosphosulfate
Electrocatalyst
Hydrogen evolution reaction

ABSTRACT

The morphology and crystallographic surface can influence the catalytic HER activity of electrocatalyst. With sufficient active sites and surface area, nanoporous materials with three-dimensional interconnected porous networks have shown the promising application in electrocatalyst. In this work, we report a simple method that can synthesize the self-supported nanoporous cobalt phosphosulfate (CoP|S) electrocatalyst. Theoretical calculation shows that the phosphorus substitution by sulfur can control the electronic structures of the active sites and accelerate charge transfer of CoP, therefore improving HER activity. The experimental study shows that nanoporous CoP|S electrodes present the improved HER performance compared with CoP in alkaline media and acidic media, respectively.

1. Introduction

Hydrogen is promising alternative energy to reduce the usage of fossil fuels and meet the demand for renewable energy. As an environmentally friendly method, electrochemically water splitting is a highly desirable way to produce clean and high-purity H₂ fuel [1–5]. The efficient massive production of H₂ mainly relies on the activity and cost of the electrocatalyst. Pt and its alloys have been well known as the best hydrogen evolution reaction (HER) catalysts [6,7]. However, the low abundance and the excessive cost of Pt severely restrict their applications in large-scale. Therefore, numerous efforts have been devoted to exploring the non-precious catalyst alternatives, including transition-metal dichalcogenides (TMDs), and phosphides, such as MoS₂ [8–10], WS₂ [11,12], MoSe₂ [13,14], CoS₂, [15] MoP [16,17], CoP [18–21], Co₂P [22,23] etc., as well as their derivatives.

As a metallic electrocatalyst, CoP has attracted intense attention for their potential of replacing expensive catalysts for electrochemical hydrogen generation. In principle, HER activity of CoP, can be further improved by increasing the exposed surface area, the activity of active sites, and manipulating the reactants transport on the electrolyte/electrode interface. The element substitution can control the electronic structures of the active sites and accelerate charge transfer to further

improve the catalytic HER activity and stability of the catalyst [24–28]. The pyrite-type ternary compound CoPS, firstly reported by Caban-Acevedo, M. et al. [29] has attracted a lot of attention due to its high intrinsic activity. Li et al., reported the metal organic framework-derived technique to anchor the CoPS nanoparticles on the nitrogen-doped carbon frameworks and provided superior electrochemical performance [30]. Coincidentally, the CoPS nanoparticles encapsulated in N, P, S tri-doped porous carbon had been prepared to improve the activity and stability [31]. Apart from the excellent performance of CoPS supported on three-dimensional porous morphology, Wu et al. [32] discovered that HER activity of CoPS also depends on the crystallographic surface, which can influence the H atom adsorption energies and barriers to H₂ desorption on the catalyst surface, thereby affecting its HER behavior. Such crystal orientation dependence of HER activity provides a direction to design of high-performance electrocatalysts.

Nanoporous materials have shown high HER activity due to its large surface area and the improvement of mass transport properties at electrolyte/electrode interface. Except for the nanoporous bimetallic material [33,34], porous TMD supported by nanoporous metal have been reported for efficient HER. The electrocatalyst of core-shell amorphous molybdenum sulfide (MoS_{2,7}) on nanoporous gold developed by Ge et al., showing high HER activity due to the interplay

* Corresponding author at: CAS Key Laboratory of Design and Assembly of Functional Nanostructures, Fujian Provincial Key Laboratory of Nanomaterials, Fujian Institute of Research on the Structure of Matter, Chinese Academy of Sciences, Fuzhou, 350002, China.

E-mail address: liuw@fjirsm.ac.cn (W. Liu).

between the thin $\text{MoS}_{2.7}$ layer and the high conductive and large surface of nanoporous gold [35]. Tan and his colleagues synthesized a large-scale 3D monolayer MoS_2 on the curved internal surface of nanoporous gold with out-of-plane strains by lattice bending, in which the 2D MoS_2 catalyst emerged a large effective surface area and high catalytic activity [36]. The mesoporous MoS_2 thin films with double-gyroid morphology synthesized by the assistance of silica template exhibit large-area and expose more active edge sites, enabling the improvement of catalytic activity [37]. However, it is worth to note that it is still lack of a method to prepare self-supported CoPS nanoporous catalyst. Therefore, it's highly desirable to design the nanoporous CoPS structure to the enhancement in the catalytic activity for HER.

Herein, we report a simple method to synthesize self-supported nanoporous CoP|S (partial of P atoms are replaced by S atoms) through a simple annealing method. The self-supported nanoporous CoP|S can significantly increase the surface area and provide abundant active sites, which improve the activity of HER performance. The nanoporous CoP|S also allow the gas diffusion efficiently to enhance mass transport properties. The electrochemistry results show that the nanoporous CoP|S electrode shows better HER performance than that of CoP . The self-supported nanoporous CoP|S electrodes present the excellent catalytic HER performance with a low overpotential of 103 mV and 107 mV at a current density of 10 mA/cm^2 in alkaline media and acidic media, respectively.

2. Experimental section

2.1. Materials synthesis

2.1.1. Synthesis of CoO/Ti

Ti foils are utilized as a substrate to prepare CoP|S electrode. Ti foils were cleaned in hydrochloric acid for 10 min to eliminate the surface oxide coating subsequently washed with deionized water, ethanol, and acetone, and dried under a stream of nitrogen. Cobalt nitrate hexahydrate ($(\text{Co}(\text{NO}_3)_2 \cdot 6\text{H}_2\text{O}$, AR, 98.5%) with a loading account of 0.1 g was dissolved in 5 ml of deionized water. After vigorous stirring at room temperature for 1 h, a light pink solution was obtained. The pink solution with $10 \mu\text{l}$ was measured using pipettor and dropped onto the surface of Ti foils uniformly. The mass loading on Ti foils was about 0.2 mg. These samples were heated at 65 °C to evaporate the water of cobalt nitrate hexahydrate solution. Follow these steps, the samples were placed in the center of a fused silica tube and heated to 350 °C for 30 min in a tube furnace at a 30 sccm argon (99.999%) flow rate. After cooling, a cobalt oxide product as CoO was produced on Ti foils.

2.1.2. Synthesis of CoP|S/Ti electrodes

To prepare CoP|S catalysts, a 2-inch diameter quartz tube furnace was used (SKGL-1200-II). In a typical synthesis, an alumina porcelain boat containing 0.6 g of a 1:1 mixture of sulfur (CP, 99.5%) and phosphorus (AR, 98.5%) powders was placed in the center of the first region of the quartz tube reactor equipped with pressure gauge and gas flow controllers. The CoO/Ti precursor substrates were placed on an alumina plate at the center of the downstream second region of the tube furnace. Firstly, the first region of the tube furnace was heated to 200 °C for 10 min with Ar carrier gas at 30 sccm. After the tube was cooled to room temperature without opening the tube to the air, the mixture of sulfur and phosphorus powders was converted to a thiophosphate (P_xS_y) paste-like product in the alumina boat. Then, the temperature of the first zone with the thiophosphate precursor was raised to 450 °C at a speed of 22 °C/min and maintained for 70 min, while the second zone in the downstream with the CoO/Ti precursor substrates was heated to 650 °C with the rate of 25 °C/min and maintained for 60 min. During growth, the tube was in an argon (30 sccm) and hydrogen gas (15 sccm, 99.999%) atmosphere. After growth, the system was cooled down to room temperature naturally.

2.1.3. Synthesis of CoP/Ti electrodes

CoP grown on Ti foil is achieved through one step of phosphorization process of CoO/Ti foil. 0.6 g of phosphorus powders was loaded in the center of the first region of the quartz tube as the phosphorus precursor and heated to 450 °C. The CoO/Ti precursor substrates were placed at the center of the downstream second region of the tube furnace and heated to 650 °C. The process was maintained for 60 min in argon at 30 sccm and hydrogen gas at 15 sccm atmospheres and then cooled down to room temperature naturally.

2.1.4. Synthesis of $\text{Co}_9\text{S}_8/\text{Ti}$ electrodes

The synthetic method of $\text{Co}_9\text{S}_8/\text{Ti}$ was the same as that for CoP/Ti as described in the preceding text except for 0.6 g of sulfur powders instead of 0.6 g of phosphorus powders was used for the precursor preparation.

2.2. Electrochemical measurement

The electrocatalytic HER performance of various electrocatalysts is tested by a typical three-electrode system on an electrochemical workstation (CHI660E). In this study, all electrochemical reactions were measured using Ag/AgCl (in 3.8 mol/L KCl solution) reference electrode at room temperature. The measurements discussed are performed in 0.5 mol/L H_2SO_4 ($\text{pH} = 0$) electrolyte and 1.0 mol/L KOH ($\text{pH} = 14$) solution electrolyte, respectively, using graphite counter electrode and converted to the reversible hydrogen electrode (RHE) unless specified. The linear sweep voltammetry scans from 0 to -0.8 V (vs. Ag/AgCl) and -1 to -1.8 V (vs. Ag/AgCl) are conducted in 0.5 M H_2SO_4 electrolyte and 1 M KOH solution, respectively. All the current density values given in the text refer to the visible area of the working electrode (1.0 cm^2). All data are collected without iR compensation.

3. Results and discussion

3.1. Morphology, and structure analysis of catalysts

The synthesis of CoP|S catalysts structures on Ti foil is achieved through a simple two-step annealing method in the experimental section. Ti foil is utilized as the conducting substrate to support CoP|S and electron collector for HER. As illustrated in Fig. 1a, CoP|S can be synthesized by the reaction of CoO with thiophosphate precursor in hydrogen and argon atmosphere at 650 °C. The CoO film is from the decomposition of cobalt nitrate hexahydrate in Ar at 350 °C (Fig. 1b). Fig. 1c shows the SEM image of CoP|S , which has coral-like nanoporous structures. A close observation of CoP|S reveals that the interconnected nanoporous CoP|S structure has large amount holes (less than 100 nm) and smooth surface.

Through the analysis of the morphology of prepared samples, we can conclude that the morphology of Co-based catalyst is determined by phosphorization and sulfurization process. Fig. S1 exhibits SEM images for different morphologies of Co-based catalyst synthesized on Ti foil after either sulfurization or phosphorization treatments. After the sulfurization, CoO can be converted into Co_9S_8 with bulk structure (Fig. S1a). For CoP catalyst, part of CoP catalyst shows a coral-like nanoporous morphology after CoO reacts with the phosphorus (Figs. S1b, 1c). Compared with the morphology of CoP|S with CoP and Co_9S_8 , hence, the sulfurization process with thiophosphate precursor may facilitate the formation of nanoporous structure.

The self-supported nanoporous CoP|S structure exposed different crystal faces, which can increase the curved surface and expose the active crystal face for HER. Compared with the single plane (Fig. 1f), the interface of (100) and (110) facets of CoP|S crystal (Fig. 1e) offers the two active sites nearby, thereby reducing the distance of the adsorbed H atoms. Hence, the recombination of the two adsorbed hydrogen atoms to form an H_2 molecule in HER would benefit from the two proximate active sites [38]. The curved geometric configuration

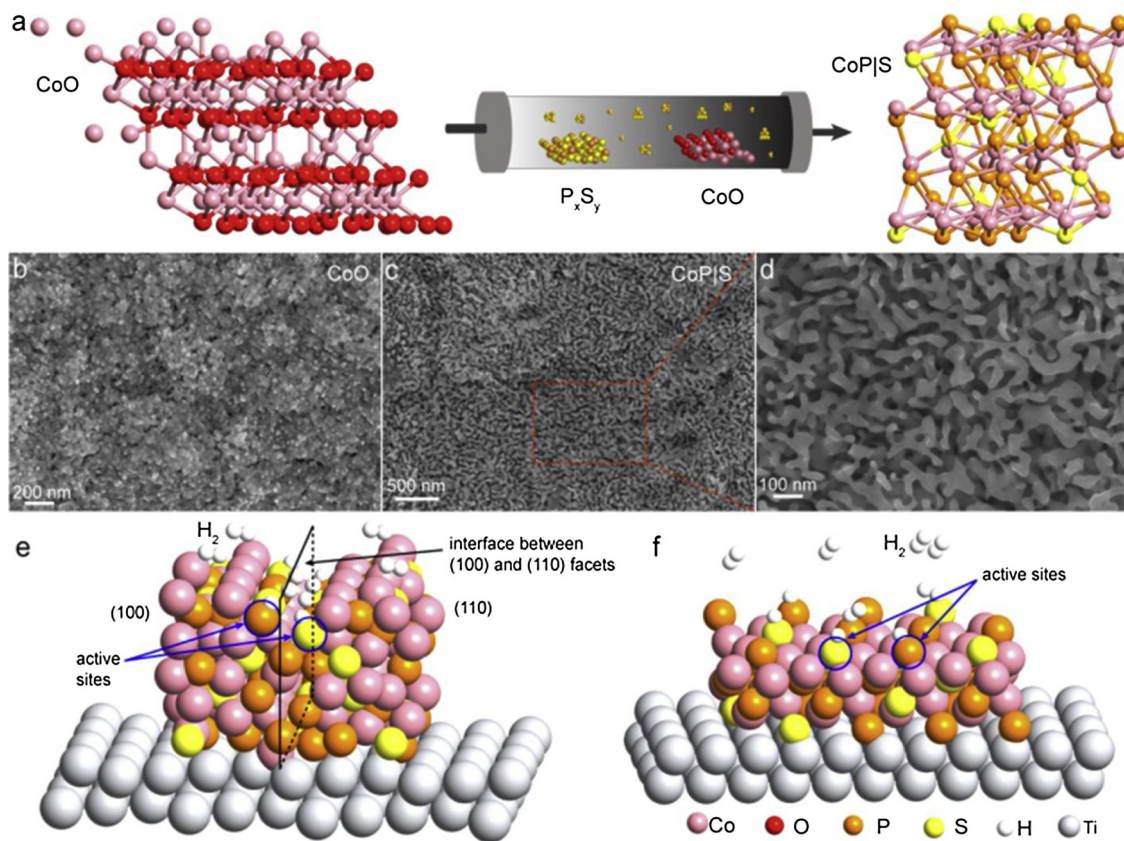


Fig. 1. (a) Schematic of the synthesis process of CoP|S through a phosphorization and sulfurization of CoO at 650 °C. (b) Scanning electron microscopy (SEM) image of CoO nanoparticles film. (c), (d) SEM image of nanoporous CoP|S. (e) A curved surface formed near the interface between (100) and (110) of CoP|S crystal. This curved surface offers active sites and reduces the distance of the H atoms. (f) An open (100) surface of CoP|S on Ti atoms. The length of two active sites is larger than that of the curved surface shown in (e).

differs from the traditional two-dimensional open surface that separates two active sites at a distance as shown in Fig. 1f. In addition, with the interconnected nanoporous structure of CoP|S, the gas bubble produced during HER can diffuse through the holes of the porous structure, therefore diminishing the impact of a gas bubble on the active sites.

HRTEM analysis is conducted to study the crystallinity of CoP|S catalyst as shown in Fig. 2a. The interplanar spacing of 0.247 nm and 0.189 nm can be assigned to the (111) and (211) facets of CoP|S crystal in Fig. 2 a1, a2, [39,40] respectively. The Dr. Probe method is used to simulate High-Angle Annular Dark Field (HAADF) images of CoP|S for (111) and (211) faces [41]. The detailed Dr. Probe calculation method is described in Supplementary Information and Fig. S2. As shown in Fig. 2b and c, the bright spots linked with orange lines in denoting the interplanar spacing. As shown in Fig. 2d, EDS elemental mapping images confirm the homogeneous distribution of Co, P and S elements in the catalyst.

The XRD pattern of CoP|S, and CoP are presented in Fig. 3a for comparison. As depicted in Fig. 3a, the XRD pattern characteristic of CoP|S agrees with the sulfur-deficient CoP structure [42,43], indicating that phosphatization is the primary reaction during the phosphatization and sulfurization process with the thiophosphate precursor. To further analyze the elemental composition of CoP|S catalyst, the corresponding energy-dispersive X-ray spectroscopy (EDX) was shown in Fig. S3. For the synthesized CoP|S, P/S atomic ratio is around 3:1, implying that ~25% of the P sites was substituted by S element (${}^{\text{C}}\text{CoP}_{0.75}\text{S}_{0.25}$). Since the similar atomic sizes for S and P, the process of substitution has a minimal influence on the crystal structure and lattice parameters of CoP as calculated in Fig. 3b [44].

Density functional theory (DFT) calculation has been carried out to estimate the characteristics of CoP|S crystal. A $2 \times 2 \times 3$ supercell

structural model of CoP and $\text{CoP}_{0.75}\text{S}_{0.25}$ with the substitution of one S element per four P elements are investigated with sufficient vacuum ($> 10 \text{ \AA}$) on z-direction. The band structures of CoP (left) and CoP|S (right) are plotted as shown in Fig. 3c, which suggest that CoP and CoP|S crystals are metallic, the conductive structure can facilitate charge transport. PDOS of CoP and CoP|S are plotted in Fig. 3d. As shown in Fig. 3d, the electron density for p orbit of S atoms is very small, and p orbit of P atom exhibits a negligible change for CoP|S and CoP, but the d orbit of Co atom for CoP|S is slightly increased compared with CoP, especially for the electron density around Fermi level. Therefore, although the substitution of sulfur for phosphorus would not influence on the crystal structure and lattice parameters, the introduction of S element could also modestly change the hybridization with the unaltered p orbit of P atom and the slightly increased d orbit of Co atom. The increased electron density in CoP|S would enhance the strength of Co-H and consequently benefits H^+ reduction [45].

The composition of CoP|S is further analyzed by XPS as shown in Figs. 3e–g and S4. The survey XPS spectrum (Fig. S4c) of the CoP|S contains the prominent peaks belonging to Co, P, S, O, C and Ti elements, the signals of C and O elements could be arise from contamination/surface oxidation due to air contact [42,46]. Fig. 3e shows that CoP|S has a binding energy of 779.4 eV, 781.7 eV, and 785.2 eV in the Co 2p core level spectrum, which correspond to Co-P in CoP|S, oxidized Co species and the satellite peaks, respectively [42,47]. As shown in Fig. 3f, S 2p core level spectrum of the CoP|S reveals the binding energy at 162.4 eV, which can be ascribed to sulfide species. The absence of sulfate species for the binding energy around 168 eV indicates the prevention of oxidation state S for phosphorization and sulfurization [44]. The binding energy of P 2p peaks for nanoporous CoP|S (Fig. 3g) located at 129.2 eV, 130.1 eV, and 133.9 eV correspond

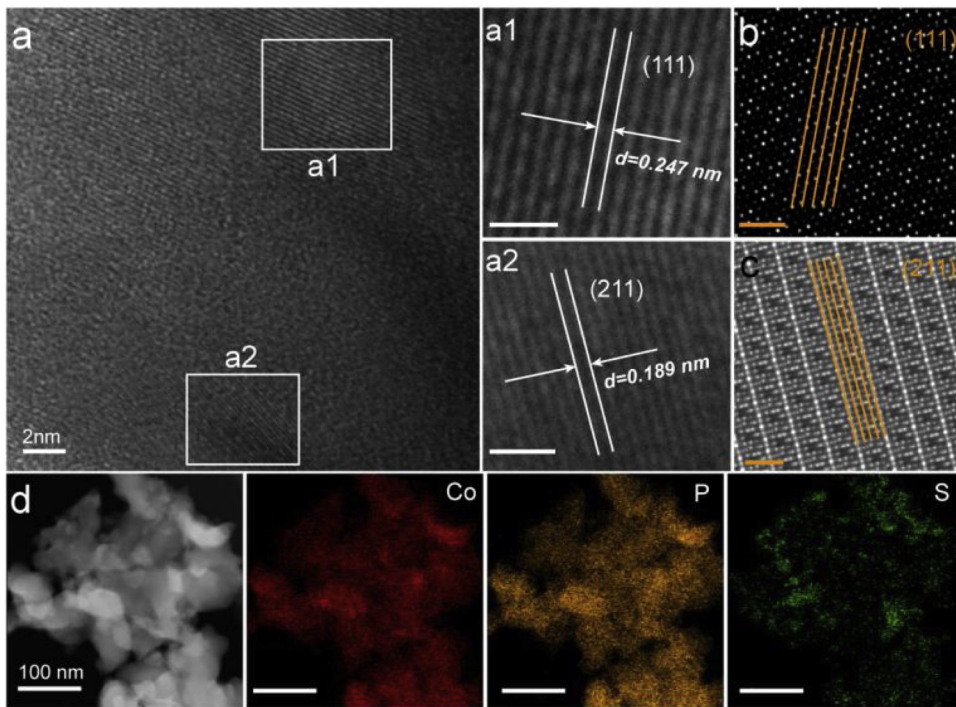


Fig. 2. (a) High-resolution transmission electron microscopy (HRTEM) image of CoP|S catalyst: (a1) (111) facet and (a2) (211) facet. (b, c) The simulated High-Angle Annular Dark Field (HAADF) images of CoP|S with (111) and (211) faces. The scale bar in (a1, a2, b, and c): 1 nm. (d) EDS elemental mapping of Co, P, and S for CoP|S electrode.

to P 2p_{3/2}, P 2p_{1/2}, and oxidized P species, respectively [42,46,48]. Beside, by comparison with O 1s peaks of CoO (Fig. S4b), the absence of the peak at 529.7 eV in the O 1s core level spectrum for CoP|S (Fig. S4d) indicates that the characteristic peak related to the contribution of O²⁻ in rocksalt and spinel metal oxides (Co₃O₄) [49,50] is completely disappeared, confirming that the CoO was fully transformed into CoP|S. The O 1s spectrum shows the existence of oxidized Co and P species. Compared with the binding energy of metallic Co (778.1 eV) and elemental phosphorus (130 eV), sulphur (164 eV), the positive shift of Co 2p_{3/2} and negative shift of P 2p_{3/2}, S 2p suggest that Co and P, S in the CoP|S catalyst have a partial positive charge (δ^+) and negative charge (δ^-), respectively, [43,51] implying the electron density transfer from Co to S and P.

3.2. Electrochemical characterization

Fig. 4 shows LSV curves of Ti foil, CoP, CoP|S, Co₉S₈ and commercial Pt/C (20 wt% Pt/XC-72) catalysts measured in 0.5 M H₂SO₄ and 1 M KOH solution. Pristine Ti foil exhibits ignorable HER activity as shown in Fig. 4a, b, while the catalytic HER activity of nanoporous CoP|S on Ti foil with a loading amounts of 0.2 mg/cm² achieve the cathodic current density of 10 mA/cm² at a low overpotential of 107 mV and 103 mV versus reversible hydrogen electrode (RHE) in 0.5 M H₂SO₄ and 1 M KOH solution, respectively. Since the nanoporous CoP|S catalyst exposes more active sites for HER, CoP|S electrode reveals a better catalytic activity than that of CoP (129 mV and 133 mV) electrode.

It's generally considered that the reaction mechanism of HER in acidic electrolyte is suggested by three steps [52–54]: First is the primary electron transfer step (Volmer reaction), $\text{H}_3\text{O}^+ + \text{M} + \text{e}^- \rightarrow \text{MH}_{\text{ads}} + \text{H}_2\text{O}$, this step is followed by either the second step of an electrochemical desorption process (Heyrovsky reaction), $\text{MH}_{\text{ads}} + \text{H}_3\text{O}^+ + \text{e}^- \rightarrow \text{M} + \text{H}_2 \uparrow + \text{H}_2\text{O}$, or the third step of a recombination process (Tafel reaction), $2\text{MH}_{\text{ads}} \rightarrow 2\text{M} + \text{H}_2 \uparrow$. To further understand HER mechanism of CoP|S catalysts, the corresponding Tafel plots are shown in Fig. 4c, d. The Tafel slope of nanoporous CoP|S is estimated to be 57 mV/dec and 58 mV/dec in 0.5 M H₂SO₄ and 1 M KOH, respectively, which is lower than that of CoP (70 mV/dec and 67 mV/dec),

suggesting the more efficient HER process on nanoporous CoP|S. The Tafel slope reveals the speed and favorable kinetics of HER catalysts. The value of nanoporous CoP|S catalyst indicates that the rate determining step can be identified as the process of electrochemical desorption, implying the Volmer-Heyrovsky mechanism, which is different from Pt/C with a Tafel slope of 29 mV/dec and 30 mV/dec (Volmer-Tafel mechanism: recombination process as the rate-determining step) in acid and alkaline media, respectively [39,54].

Additionally, the stability test of nanoporous CoP|S is also measured to study the stability of electrocatalyst in evaluating HER performance. Continuous cyclic voltammetry (CV) test with 1000 cycles is carried out to acquire the long-term stability of nanoporous CoP|S electrodes in the 0.5 M H₂SO₄ and 1 M KOH media, as shown in Fig. 4e, f. Compared with their initial activities, the current density of nanoporous CoP|S exhibits a negligible change after 1000 cycles in acidic media, while continuous CV test in alkaline electrolyte demonstrates a slight attenuation of current density for nanoporous CoP|S electrode after 1000 cycles. Insets of Fig. 4e, f show that the catalytic activities of the CoP|S catalyst could be retained for 25 h at the constant overpotentials to get the current density around 10 mA/cm² both in acidic and alkaline electrolytes. The electrocatalyst demonstrates excellent stability in comparison with the initial currents after operation for 25 h in acidic and alkaline electrolytes, respectively, exhibiting its potential application in the process of H₂ production. Fig. S5 shows the SEM and XPS images of CoP|S/Ti after stability test in acidic and alkaline media. In addition, we further analyzed the gaseous products generated upon electrocatalysis by gas chromatography (GC). The Faradic efficiency was calculated by the comparison of the amount of experimentally measured hydrogen with theoretically calculated hydrogen. As shown in Fig. S6, the CoP|S catalysts afforded nearly 100% Faradaic yield at -0.15 V vs. RHE in acidic media and at -0.34 V vs. RHE in alkaline media, confirming the current density came from the hydrogen generation.

The electrochemical effective surface area (ECSA) is another critical factor for catalyst in HER process, as it is well known that the larger ECSA is responsible for the enhanced catalytic activity [55]. The capacitance of electrochemical double-layer (C_{dl}) is used to explain the ECSA, which can be determined by the CV curves in both acid and

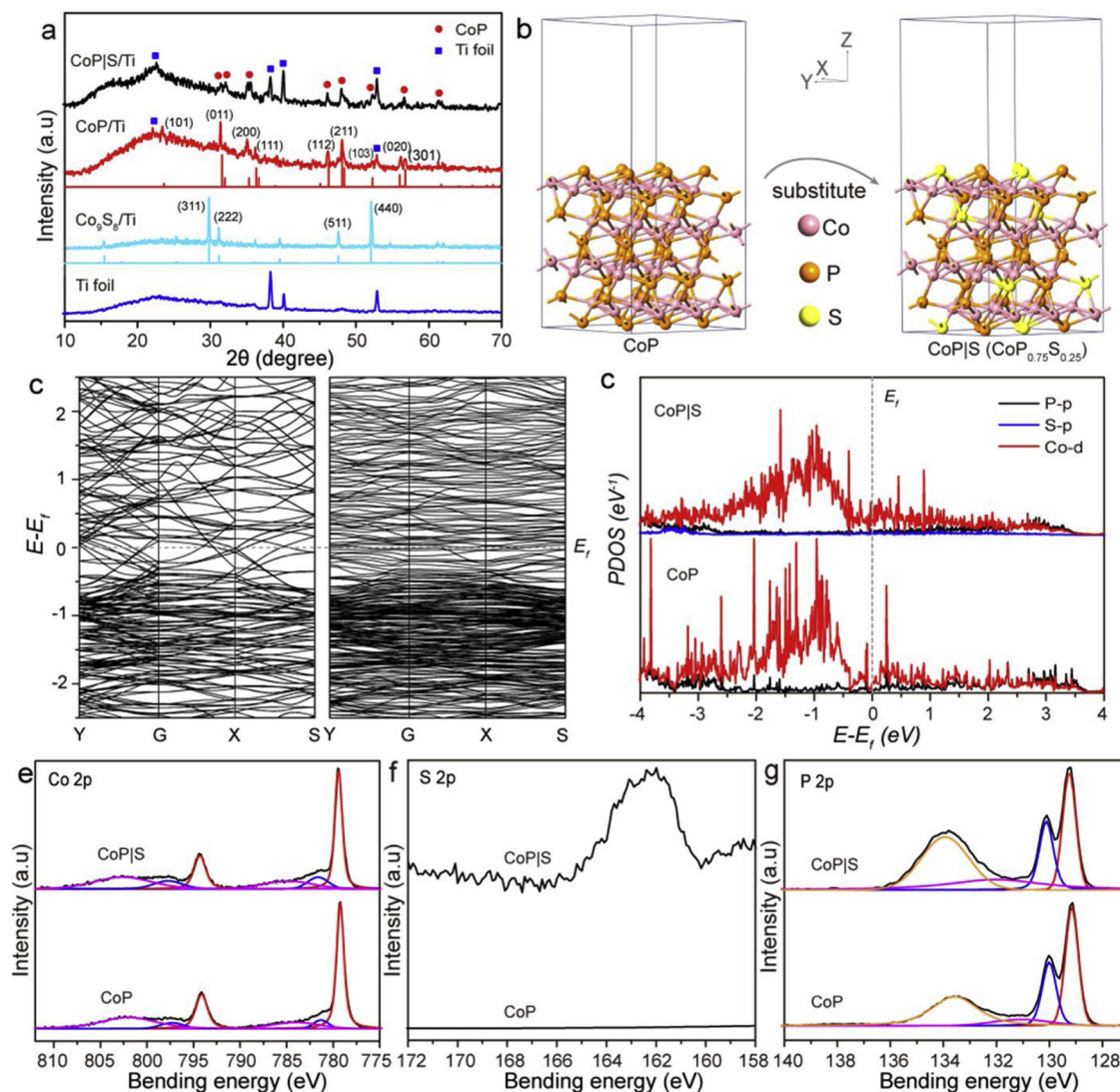


Fig. 3. (a) XRD pattern of CoP|S, CoP and Co₉S₈ measured on Ti substrates. (b) The unit cell of CoP and CoP|S. The substitution of sulfur for phosphorus could happen without an influence on the crystal structure and lattice parameters. (c) The band structure for CoP (left) and CoP|S (right). (d) The projected density of state (PDOS) for CoP and CoP|S crystals. X-ray photoelectron spectroscopy (XPS) spectra of (e) Co 2p, (f) S 2p and (g) P 2p peaks of CoP|S.

alkaline electrolytes, as shown in Figs. S7 and S8, respectively. The scan rates are set in the range of 10–90 mV/s with an interval of 10 mV/s. As shown in Fig. S9a and b, C_{dl} is one half of the linear slope of fitted lines of the plots in the figure of Δj against the CV scan rates, where Δj is the difference between the negative current density and positive current density in CV curves at a given potential of 0.285 V vs. RHE in 0.5 M H₂SO₄ solution and at 0.626 V vs. RHE in 1 M KOH, respectively.

Ti foil shows a negligible value of C_{dl} (0.88 m F/cm² in 0.5 M H₂SO₄ and 0.89 m F/cm² in 1 M KOH). The C_{dl} value is calculated to be 12.71 m F/cm² and 12.48 m F/cm² for nanoporous CoP|S in 0.5 M H₂SO₄ solution and in 1 M KOH environment, respectively, which is much larger than that of CoP catalyst (10.90 m F/cm² and 10.85 m F/cm²). The larger value of C_{dl} for nanoporous CoP|S indicates the larger specific surface area to support abundant active sites for the higher HER catalytic activity, which is consistent with the phenomenon of SEM images in Fig. 1c–d and the observed activity in Fig. 4.

Moreover, the interface behavior of the CoP|S electrodes is also measured by electrochemical impedance spectroscopy (EIS). The typical Nyquist plots of the EIS response to various samples are obtained at the given potentials of −0.35 V and −1.15 V in 0.5 M H₂SO₄ and 1 M KOH solution, respectively, as depicted in Fig. S9c and d. Inset of Fig. S9c and d show the corresponding equivalent circuit model comprising

a solution resistance (R_s) and the parallel combination of a constant phase element (CPE) and a charge transfer resistance (R_{ct}). The semi-circle in the Nyquist plots can be used to describe R_{ct} and is inversely proportional to the conductivity of catalyst. From the semicircle Nyquist plots, Ti foil and Co₉S₈ exhibit large values both in acidic and alkaline media, indicating their poor activities at the given potentials. As compared to CoP whose R_s and R_{ct} values are 5.83 and 53.87 Ω, respectively, CoP|S has more significant value of R_s of 11.28 Ω but much smaller value R_{ct} of 34.08 Ω in 0.5 M H₂SO₄. Similarly, in alkaline media, CoP shows the values of R_s and R_{ct} of 12.98 and 66.13 Ω, respectively, CoP|S obtains smaller values of R_s and R_{ct} of 11.91 and 32.98 Ω, respectively. The smaller radii of semicircles suggest the more efficient electron charge transfer of HER on the surface of CoP|S that could devote to the superior HER kinetics. The smallest charge transfer resistance for CoP|S may be contributed to the diffusion channels with the steady movement of the gas bubble and the interconnected conductive network for electron transport in nanoporous CoP|S structure.

3.3. DFT calculation

According to HRTEM and XRD of CoP|S mentioned above, the (211)

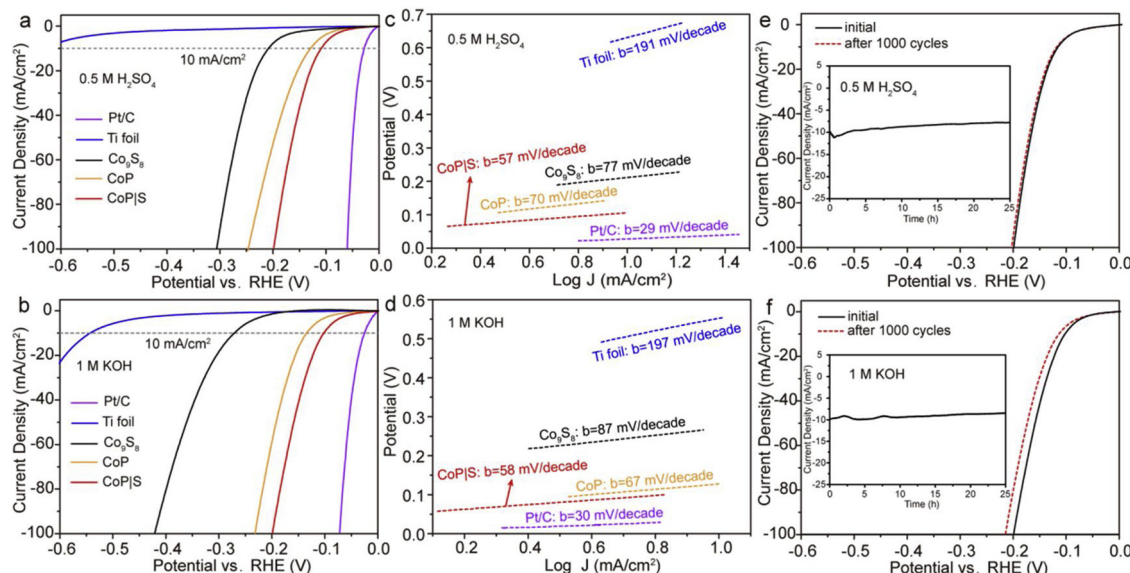
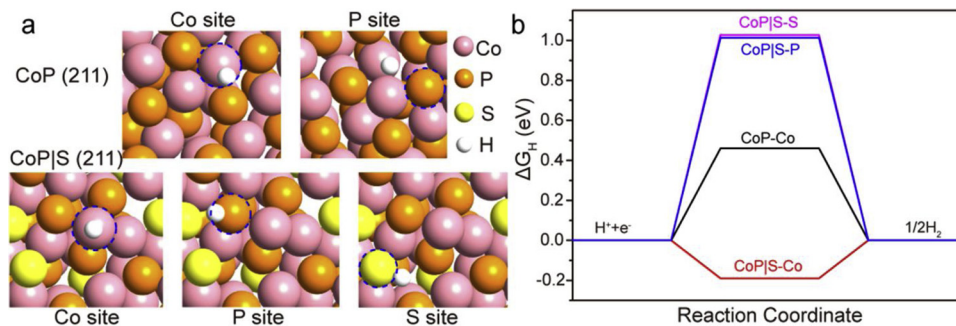


Fig. 4. (a, b) Linear sweep voltammetry (LSV) curves and (c, d) the corresponding Tafel plots of Ti foil, CoP, CoP|S, Co₉S₈ and commercial Pt/C catalysts measured in 0.5 M H₂SO₄ and 1 M KOH solution, respectively. (e, f) LSV curves of CoP|S catalyst before (black curve) and after 1000 cycles (red curve) of cyclic voltammetry stability test in 0.5 M H₂SO₄ and 1 M KOH solution, respectively. The insets in (e) and (f) show the time dependence of the current density for nanoporous CoP|S catalyst while being held at the constant external potentials to get the current density around 10 mA/cm² in 0.5 M H₂SO₄ and 1 M KOH electrolyte for 25 h, respectively (For interpretation of the references to colour in this figure legend, the reader is referred to the web version of this article).



surface is the dominant crystal surface exposed in the synthesized CoP|S catalyst. The possible surface atom features adsorbed H atom of nanoporous CoP|S (211) and CoP (211) at Co site, P site or S site are optimized as displayed in Fig. 5a. The optimized results suggest that hydrogen atom adsorbed at P site for CoP is unstable since the hydrogen atom in its optimized structure tends towards adsorbing at Co site [56].

Gibbs free energy for hydrogen adsorption (ΔG_H) at Co site, P site and S site for CoP|S (211) in comparison to at Co site for CoP (211) is calculated to evaluate the hydrogen evolution activity, as shown in Fig. 5b. The ΔG_H value at Co site for the CoP catalyst is 0.46 eV. CoP|S exhibits favorable catalyst-H energetics at Co site, exhibiting a very small activated H adsorption energy down to -0.19 eV, much smaller than those values at P site or S site around ~ 1 eV. The adsorption at Co site is found to be favorable than at Co site in CoP, indicating that the electronic structure modified by the substitution of sulfur for phosphorus can enhance the catalyst activity for HER, even though the crystal structure and lattice parameters could not be affected.

4. Conclusions

In conclusion, we develop a simple process to prepare self-supported nanoporous CoP|S catalysts on Ti foil. The substitution of sulfur for phosphorus not only facilitates the formation of nanoporous structure to increase the surface area and supply abundant active sites but slightly modifies the electronic structure, therefore boosting the

catalyst activity of CoP|S for HER. Nanoporous CoP|S catalyst provides the excellent catalytic HER performance with a low overpotential of 107 mV and 103 mV at a current density of 10 mA/cm² in 0.5 M H₂SO₄ and 1 M KOH electrolyte, respectively. This work provides a straightforward method to prepare nanoporous CoP|S electrodes towards the high efficient water splitting at low cost.

Acknowledgments

This work was supported by Fujian Institute of Research on the Structure of Matter, Chinese Academy of Sciences, the National Natural Science Foundation of China (No. 61674152), and the Natural Science Foundation of Fujian Province of China (No. 2017J01130).

Appendix A. Supplementary data

Supplementary material related to this article can be found, in the online version, at doi:<https://doi.org/10.1016/j.apcatb.2019.03.070>.

References

- [1] M.S. Dresselhaus, I.L. Thomas, Alternative energy technologies, *Nature* 414 (2001) 332–337.
- [2] C. Jian, Q. Cai, W. Hong, J. Li, W. Liu, Enhanced hydrogen evolution reaction of MoO_x/Mo cathode by loading small amount of Pt nanoparticles in alkaline solution, *Int. J. Hydrogen Energy* 42 (2017) 17030–17037.
- [3] J.O.M. Bockris, The origin of ideas on a Hydrogen Economy and its solution to the

decay of the environment, *Int. J. Hydrogen Energy* 27 (2002) 731–740.

[4] H. Yang, Y. Zhang, F. Hu, Q. Wang, Urchin-like CoP nanocrystals as hydrogen evolution reaction and oxygen reduction reaction dual-electrocatalyst with superior stability, *Nano Lett.* 15 (2015) 7616–7620.

[5] X. Zhang, X. Zhang, H. Xu, Z. Wu, H. Wang, Y. Liang, Iron-doped cobalt monophosphide nanosheet/carbon nanotube hybrids as active and stable electrocatalysts for water splitting, *Adv. Funct. Mater.* 27 (2017) 1606635.

[6] J.K. Norskov, T. Bligaard, J. Rossmeisl, C.H. Christensen, Towards the computational design of solid catalysts, *Nat. Chem.* 1 (2009) 37–46.

[7] W. Sheng, H.A. Gasteiger, Y. Shao-Horn, Hydrogen oxidation and evolution reaction kinetics on platinum: acid vs alkaline electrolytes, *J. Electrochem. Soc.* 157 (2010) B1529–B1536 8.

[8] H. Zhu, G. Gao, M. Du, J. Zhou, K. Wang, W. Wu, Xu Chen, Y. Li, P. Ma, W. Dong, F. Duan, M. Chen, G. Wu, J. Wu, H. Yang, S. Guo, Atomic-scale core/shell structure engineering induces precise tensile strain to boost hydrogen evolution catalysis, *Adv. Mater.* 30 (2018) 1707301.

[9] J. Hu, B. Huang, C. Zhang, Z. Wang, Y. An, D. Zhou, H. Lin, M.K.H. Leung, S. Yang, Engineering stepped edge surface structures of MoS₂ sheet stacks to accelerate the hydrogen evolution reaction, *Synth. Lect. Energy Environ. Technol. Sci. Soc.* 10 (2017) 593–603.

[10] J. Li, J. Kang, Q. Cai, W. Hong, C. Jian, W. Liu, K. Banerjee, Boosting hydrogen evolution performance of MoS₂ by band structure engineering, *Adv. Mater. Interfaces* 4 (2017) 1700303.

[11] J. Duan, S. Chen, B.A. Chambers, G.G. Andersson, S.Z. Qiao, 3D WS₂ Nanolayers@Heteroatom-doped graphene films as hydrogen evolution catalyst electrodes, *Adv. Mater.* 27 (2015) 4234–4241.

[12] J. Li, W. Hong, C. Jian, Q. Cai, W. Liu, Seamless tungsten disulfide-tungsten heterojunction with abundant exposed active sites for efficient hydrogen evolution, *Appl. Catal. B: Environ.* 244 (2019) 320–326.

[13] Y. Yin, Y. Zhang, T. Gao, T. Yao, X. Zhang, J. Han, X. Wang, Z. Zhang, P. Xu, P. Zhang, X. Cao, Bo Song, S. Jin, Synergistic phase and disorder engineering in 1T-MoS₂ nanosheets for enhanced hydrogen-evolution reaction, *Adv. Mater.* 29 (2017) 1700311.

[14] C. Jian, Q. Cai, W. Hong, J. Li, W. Liu, Edge-riched MoSe₂/MoO₃ hybrid electrocatalyst for efficient hydrogen evolution reaction, *Small* 14 (2018) 1703798.

[15] M.S. Faber, R. Dziedzic, M.A. Lukowski, N.S. Kaiser, Q. Ding, S. Jin, High-performance electrocatalysis using metallic cobalt pyrite (CoS₂) Micro- and nanostructures, *J. Am. Chem. Soc.* 136 (2014) 10053–10061.

[16] J. Kibsgaard, T.F. Jaramillo, Molybdenum phosphosulfide: an active, acid-stable, earth-abundant catalyst for the hydrogen evolution reaction, *Angew. Chem. Int. Ed.* 53 (2014) 14433–14437.

[17] G. Zhang, G. Wang, Y. Liu, H. Liu, J. Qu, J. Li, Highly active and stable catalysts of phytic acid-derivative transition metal phosphides for full water splitting, *J. Am. Chem. Soc.* 138 (2016) 14686–14693.

[18] M. Sun, H. Liu, J. Qu, J. Li, Earth-rich transition metal phosphide for energy conversion and storage, *Adv. Energ. Mater.* 6 (2016) 1600087.

[19] C. Wu, Y. Yang, D. Dong, Y. Zhang, J. Li, In situ coupling of CoP polyhedrons and carbon nanotubes as highly efficient hydrogen evolution reaction electrocatalyst, *Small* 13 (2017) 1602873.

[20] K. Wu, Z. Chen, W.C. Cheong, S. Liu, W. Zhu, X. Cao, K. Sun, Y. Lin, L. Zheng, W. Yan, Y. Pan, D. Wang, Q. Peng, C. Chen, Y. Li, Toward bifunctional overall water splitting electrocatalyst: general preparation of transition metal phosphide nanoparticles decorated N-doped porous carbon spheres, *ACS Appl. Mater. Interfaces* 10 (2018) 44201–44208.

[21] J. Song, J. Xiang, C. Mu, B. Wang, F. Wen, C. Su, C. Wang, Z. Liu, Facile synthesis and excellent electrochemical performance of CoP nanowire on carbon cloth as bifunctional electrode for hydrogen evolution reaction and supercapacitor, *Sci. China Mater.* 60 (2017) 1179–1186.

[22] J.F. Callejas, C.G. Read, E.J. Popczun, J.M. McEnaney, R.E. Schaak, Nanostructured Co₂P electrocatalyst for the hydrogen evolution reaction and direct comparison with morphologically equivalent CoP, *Chem. Mater.* 27 (2015) 3769–3774.

[23] S. Li, G. Zhang, X. Tu, J. Li, Polycrystalline CoP/CoP₂ structures for efficient full water splitting, *Chem. Electro. Chem.* 5 (2018) 701–707.

[24] T. Liu, D. Liu, F. Qu, D. Wang, L. Zhang, R. Ge, S. Hao, Y. Ma, G. Du, A.M. Asiri, L. Chen, X. Sun, Enhanced electrocatalysis for energy-efficient hydrogen production over CoP catalyst with Nonelectroactive Zn as a promoter, *Adv. Energ. Mater.* 7 (2017) 1700020.

[25] H. Du, R.M. Kong, X. Guo, F. Qu, J. Li, Recent progress in transition metal phosphides with enhanced electrocatalysis for hydrogen evolution, *Nanoscale* 10 (2018) 21617–21624.

[26] B. Ma, Z. Yang, Y. Chen, Z. Yuan, Nickel cobalt phosphide with three-dimensional nanostructure as a highly efficient electrocatalyst for hydrogen evolution reaction in both acidic and alkaline electrolytes, *Nano Res.* 12 (2019) 375–380.

[27] X. Zhang, W. Gu, E. Wang, Self-supported ternary Co_{0.5}Mn_{0.5}P/carbon cloth (CC) as a high-performance hydrogen evolution electrocatalyst, *Nano Res.* 10 (2017) 1001–1009.

[28] J. Li, Z. Xia, X. Zhou, Y. Qin, Y. Ma, Y. Qu, Quaternary pyrite-structured nickel/cobalt phosphosulfide nanowires on carbon cloth as efficient and robust electrodes for water electrolysis, *Nano Res.* 10 (2017) 814–825.

[29] M. Cabán-Acevedo, M.L. Stone, J.R. Schmidt, J.G. Thomas, Q. Ding, H.C. Chang, M. Tsai, J. He, S. Jin, Efficient hydrogen evolution catalysis using ternary pyrite-type cobalt phosphosulfide, *Nat. Mater.* 14 (2015) 1245.

[30] Y. Li, S. Niu, D. Rakov, Y. Wang, M. Cabán-Acevedo, S. Zheng, B. Song, P. Xu, Metal organic framework-derived CoPS/N-doped carbon for efficient electrocatalytic hydrogen evolution, *Nanoscale* 10 (2018) 7291–7297.

[31] Y. Hu, F. Li, Y. Long, H. Yang, L. Gao, X. Long, H. Hu, N. Xu, J. Jin, J. Ma, Ultrafine CoPS nanoparticles encapsulated in N, P, and S tri-doped porous carbon as an efficient bifunctional water splitting electrocatalyst in both acid and alkaline solutions, *J. Mater. Chem. A* 6 (2018) 10433–10440.

[32] T. Wu, M.L. Stone, M.J. Shearer, M.J. Stolt, I.A. Guzei, R.J. Hamers, R. Lu, K. Deng, S. Jin, J.R. Schmidt, Crystallographic facet dependence of the hydrogen evolution reaction on CoPS: theory and experiments, *ACS Catal.* 8 (2018) 1143–1152.

[33] Q. Lu, G.S. Hutchings, W. Yu, Y. Zhou, R.V. Forest, R. Tao, J. Rosen, B.T. Yonemoto, Z. Cao, H. Zheng, J.Q. Xiao, F. Jiao, J.G. Chen, Highly porous non-precious bimetallic electrocatalysts for efficient hydrogen evolution, *Nat. Commun.* 6 (2015) 6567.

[34] E.E. Benn, B. Gaskey, J.D. Erlebacher, Suppression of hydrogen evolution by oxygen reduction in nanoporous electrocatalysts, *J. Am. Chem. Soc.* 139 (2017) 3663–3668.

[35] X. Ge, L. Chen, L. Zhang, Y. Wen, A. Hirata, M. Chen, Nanoporous metal enhanced catalytic activities of amorphous molybdenum sulfide for high-efficiency hydrogen production, *Adv. Mater.* 26 (2014) 3100–3104.

[36] Y. Tan, P. Liu, L. Chen, W. Cong, Y. Ito, J. Han, X. Guo, Z. Tang, T. Fujita, A. Hirata, M.W. Chen, Monolayer MoS₂ films supported by 3D nanoporous metals for high-efficiency electrocatalytic hydrogen production, *Adv. Mater.* 26 (2014) 8023–8028.

[37] J. Kibsgaard, Z. Chen, B.N. Reinecke, T.F. Jaramillo, Engineering the surface structure of MoS₂ to preferentially expose active edge sites for electrocatalysis, *Nat. Mater.* 11 (2012) 963.

[38] W. Luc, F. Jiao, Nanoporous metals as electrocatalysts: state-of-the-art, opportunities, and challenges, *ACS Catal.* 7 (2017) 5856–5861.

[39] E.J. Popczun, C.G. Read, C.W. Roske, N.S. Lewis, R.E. Schaak, Highly active electrocatalysis of the hydrogen evolution reaction by cobalt phosphide nanoparticles, *Angew. Chem. Int. Ed.* 53 (2014) 5427–5430.

[40] Y. Pan, K. Sun, S. Liu, X. Cao, K. Wu, W.C. Cheong, Z. Chen, Y. Wang, Y. Li, Y. Liu, D. Wang, Q. Peng, C. Chen, Y. Li, Core-shell ZIF-8@ZIF-67-Derived CoP nanoparticle-embedded N-doped carbon nanotube hollow polyhedron for efficient overall water splitting, *J. Am. Chem. Soc.* 140 (2018) 2610–2618.

[41] J. Barthel, Dr. Probe: a software for high-resolution STEM image simulation, *Ultramicroscopy* 193 (2018) 1–11.

[42] M. Liu, J. Li, Cobalt phosphide hollow polyhedron as efficient bifunctional electrocatalysts for the evolution reaction of hydrogen and oxygen, *ACS Appl. Mater. Interfaces* 8 (2016) 2158–2165.

[43] Y.P. Zhu, Y.P. Liu, T.Z. Ren, Z.Y. Yuan, Self-supported cobalt phosphide mesoporous nanorod arrays: a flexible and bifunctional electrode for highly active electrocatalytic water reduction and oxidation, *Adv. Funct. Mater.* 25 (2015) 7337–7347.

[44] W. Liu, E. Hu, H. Jiang, Y. Xiang, Z. Weng, M. Li, Q. Fan, X. Yu, E.I. Altman, H. Wang, A highly active and stable hydrogen evolution catalyst based on pyrite-structured cobalt phosphosulfide, *Nat. Commun.* 7 (2016) 10771.

[45] H. Lin, Z. Shi, S. He, X. Yu, S. Wang, Q. Gao, Y. Tang, Heteronanowires of MoC-Mo₂C as efficient electrocatalysts for hydrogen evolution reaction, *Chem. Science* 7 (2016) 3399–3405.

[46] T. Liu, K. Wang, G. Du, A.M. Asiri, X. Sun, Self-supported CoP nanosheet arrays: a non-precious metal catalyst for efficient hydrogen generation from alkaline NaBH₄ solution, *J. Mater. Chem. A Mater. Energy Sustain.* 4 (2016) 13053–13057.

[47] Y. Cheng, F. Liao, W. Shen, L. Liu, B. Jiang, Y. Li, M. Shao, Carbon cloth supported cobalt phosphide as multifunctional catalysts for efficient overall water splitting and zinc-air batteries, *Nanoscale* 9 (2017) 18977–18982.

[48] L. Ai, Z. Niu, J. Jiang, Mechanistic insight into oxygen evolution electrocatalysis of surface phosphate modified cobalt phosphide nanorod bundles and their superior performance for overall water splitting, *Electrochim. Acta* 242 (2017) 355–363.

[49] M.M. Natile, A. Glisenti, New NiO/Co₃O₄ and Fe₂O₃/Co₃O₄ nanocomposite catalysts: synthesis and characterization, *Chem. Mater.* 15 (2003) 2502–2510.

[50] J.H. Zhong, A.L. Wang, G.R. Li, J.W. Wang, Y.N. Ou, Y.X. Tong, Co₃O₄/Ni(OH)₂ composite mesoporous nanosheet networks as a promising electrode for supercapacitor applications, *J. Mater. Chem.* 22 (2012) 5656–5665.

[51] J. Tian, Q. Liu, A.M. Asiri, X. Sun, Self-supported nanoporous cobalt phosphide nanowire arrays: an efficient 3D hydrogen-evolving cathode over the wide range of pH 0–14, *J. Am. Chem. Soc.* 136 (2014) 7587–7590.

[52] Y. Li, H. Wang, L. Xie, Y. Liang, G. Hong, H. Dai, MoS₂ nanoparticles grown on graphene: an advanced catalyst for the hydrogen evolution reaction, *J. Am. Chem. Soc.* 133 (2011) 7296–7299.

[53] J.K. Norskov, T. Bligaard, A. Logadottir, J.R. Kitchin, J.G. Chen, S. Pandelov, U. Stimming, Trends in the exchange current for hydrogen evolution, *J. Electrochem. Soc.* 152 (2005) J23–J26.

[54] Y. Shi, Y. Zhou, D.R. Yang, W.X. Xu, C. Wang, F.B. Wang, J.J. Xu, X.H. Xia, H.Y. Chen, Energy level engineering of MoS₂ by transition-metal doping for accelerating hydrogen evolution reaction, *J. Am. Chem. Soc.* 139 (2017) 15479–15485.

[55] Y.R. Zheng, P. Wu, M.R. Gao, X.L. Zhang, F.Y. Gao, H.X. Ju, R. Wu, Q. Gao, R. You, W.X. Huang, S.J. Liu, S.W. Hu, J. Zhu, Z. Li, S.H. Yu, Doping-induced structural phase transition in cobalt diselenide enables enhanced hydrogen evolution catalysis, *Nat. Commun.* 9 (2018) 2533.

[56] C. Tang, L. Gan, R. Zhang, W. Lu, X. Jiang, A.M. Asiri, X. Sun, J. Wang, L. Chen, Ternary Fe_xCo_{1-x}P nanowire array as a robust hydrogen evolution reaction electrocatalyst with Pt-like activity: experimental and theoretical insight, *Nano Lett.* 16 (2016) 6617–6621.